The 2002 Denali Fault Earthquake, Alaska: A Large Magnitude, Slip-Partitioned Event

Donna Eberhart-Phillips, *et al.*

Science **300**, 1113 (2003);
DOI: 10.1126/science.1082703

The 2002 Denali Fault Earthquake, Alaska: A Large Magnitude, Slip-Partitioned Event

Donna Eberhart-Phillips,[1] Peter J. Haeussler,[1] Jeffrey T. Freymueller,[2] Arthur D. Frankel,[3] Charles M. Rubin,[4] Patricia Craw,[5] Natalia A. Ratchkovski,[2] Greg Anderson,[6] Gary A. Carver,[7] Anthony J. Crone,[3] Timothy E. Dawson,[8] Hilary Fletcher,[2] Roger Hansen,[2] Edwin L. Harp,[3] Ruth A. Harris,[8] David P. Hill,[8] Sigrún Hreinsdóttir,[2] Randall W. Jibson,[3] Lucile M. Jones,[6] Robert Kayen,[8] David K. Keefer,[8] Christopher F. Larsen,[2] Seth C. Moran,[1] Stephen F. Personius,[3] George Plafker,[8] Brian Sherrod,[9] Kerry Sieh,[10] Nicholas Sitar,[11] Wesley K. Wallace[2]

The M_W (moment magnitude) 7.9 Denali fault earthquake on 3 November 2002 was associated with 340 kilometers of surface rupture and was the largest strike-slip earthquake in North America in almost 150 years. It illuminates earthquake mechanics and hazards of large strike-slip faults. It began with thrusting on the previously unrecognized Susitna Glacier fault, continued with right-slip on the Denali fault, then took a right step and continued with right-slip on the Totschunda fault. There is good correlation between geologically observed and geophysically inferred moment release. The earthquake produced unusually strong distal effects in the rupture propagation direction, including triggered seismicity.

Long strike-slip faults are common features of continental plate boundaries such as the San Andreas system in California, the North Anatolian system in Turkey, and the Altyn Tagh system in Asia, and they produce the largest shallow earthquakes outside of subduction zones. Worldwide, many such faults cut through heavily populated areas and are severe earthquake hazards, but few large-magnitude ($M \geq 7.5$) strike-slip earthquakes have been studied with modern instrumentation. The Denali fault is an active intracontinental right-lateral strike-slip fault that accommodates a fraction of the oblique collision of the Yakutat block into the southern Alaska margin (*1*) (Fig. 1). It is the northern boundary of a region being extruded to the west (*2*, *3*). The Totschunda fault splays off the Denali fault and strikes 14° more to the southeast. The Totschunda fault is parallel to and aligned with the plate-bounding Queen Charlotte–Fairweather transform fault system further south, and it may be part of a developing connection between the Fairweather and western Denali faults (*4*). The Alaska Range is adjacent to the Denali fault, and the high topography of the range may be related to thrust faults that merge into the Denali fault at depth (*5*, *6*).

Offsets of poorly dated Quaternary features suggest the Denali fault slip rate is 8 to 13 mm/year (*7*). GPS data indicate 8 to 9 mm/year slip on the Denali fault system, with some slip likely on parallel strands north of the main fault trace (*8*). East of the junction with the Totschunda fault, the slip rate on the Denali fault decreases to 2 to 3 mm/year (*9*). Geodetic measurements across the Totschunda fault show shear strain consistent with ~5 mm/year of dextral slip, and stream drainages offset by both the Denali and Totschunda fault systems have similar magnitudes of offset during the Quaternary (*7*).

[1]U.S. Geological Survey, 4200 University Drive, Anchorage, AK 99508, USA. [2]Geophysical Institute, University of Alaska, Fairbanks, Post Office Box 757320, Fairbanks, AK 99775-7320, USA. [3]U.S. Geological Survey, MS 966, Box 25046, Denver, CO 80225, USA. [4]Department of Geological Sciences, Central Washington University, Ellensburg, WA 98926, USA. [5]Alaska Division of Geological and Geophysical Surveys, 794 University Avenue, Suite 200, Fairbanks, AK 99709, USA. [6]U.S. Geological Survey, 525 South Wilson Avenue, Pasadena, CA 91106, USA. [7]Humboldt State University and Carver Geologic, Post Office Box 52, Kodiak, AK 99615, USA. [8]U.S. Geological Survey, 345 Middlefield Road, Menlo Park, CA 94025, USA. [9]U.S. Geological Survey, U.S. Geological Survey at Department of Earth and Space Sciences, University of Washington, Seattle, WA 98195–1310, USA. [10]Division of Geological and Planetary Sciences 100-23, California Institute of Technology, Pasadena, CA 91106, USA. [11]Department of Civil and Environmental Engineering, 441 Davis Hall, University of California, Berkeley, CA 94720, USA.

The earthquake history of the Denali fault is poorly known. Geologic studies found 6 to 8 m of slip in the last (undated) earthquake on the fault (*10*, *11*). On the basis of geotechnical studies, the Trans Alaska Pipeline at the Denali fault crossing was engineered to withstand 6.1 m of horizontal offset, 1.5 m of vertical offset, and accelerations of 0.36*g* (*12*, *13*). The part of the Denali fault west of the Totschunda fault as well as the Totschunda fault were assigned high hazard in probabilistic seismic hazard maps of Alaska on the basis of their high slip rates (*14*) (Fig. 1).

Earthquake Sequence

The Denali fault earthquake sequence began with the moment magnitude (M_W) 6.7 Nenana Mountain earthquake on 23 October 2002 (Fig. 2). This event was followed by numerous aftershocks that defined a 45-km-long zone along the Denali fault. The aftershock zone terminates ~10 km west of the subsequent M_W 7.9 epicenter. The focal mechanism shows right-lateral strike-slip, consistent with rupture on the Denali fault. Small rockfalls and snow avalanches were abundant adjacent to the Denali fault trace, but no surface slip was observed during aerial reconnaissance.

On 3 November, the 2002 M_W 7.9 Denali fault earthquake nucleated ~22 km east of the M_W 6.7 foreshock (*15*). Rupture occurred along three faults: the Susitna Glacier, Denali, and Totschunda (Fig. 2). The initial rupture of the Denali fault earthquake had a first-motion focal mechanism (Fig. 2), showing slightly oblique thrusting on a 48° north-dipping plane trending east-northeast (N82°E). This is consistent with initiation on the previously unrecognized Susitna Glacier fault. Scarps seen on aerial photos suggest one or two previous Holocene events on the Susitna Glacier thrust fault, and the westward extension of the Susitna Glacier fault beyond the rupture of 2002 is unknown.

Static stress changes from one rupture may influence subsequent ruptures (*16*, *17*). Estimated Coulomb stress increases from the M_W 6.7 event are 10 to 50 kPa on the Susitna Glacier fault and 50 to 100 kPa on the Denali fault; the ranges reflect uncertainties in event location, rupture geometry, and rheological parameters (*18*). Coulomb stress changes as low as 10 to 20 kPa, and perhaps less, are associated with earthquake triggering (*16*, *17*, *19*), consistent with Coulomb triggering of the M_W 7.9 mainshock by the M_W 6.7 foreshock. Normal stress changes are important for dip-slip faults (*20*). The M_W 6.7 event caused large extensional normal stress changes (encouraging rupture) of 100 to 150 kPa along the western Susitna Glacier fault, but

only slight (<10 kPa) compressional normal stress changes (inhibiting rupture) near the M_W 7.9 hypocenter. Thus, normal stress changes may have played a role in rupture progression but were less important for rupture initiation.

Surface rupture of three faults. The principal surface rupture accompanying the Denali Fault earthquake is a 218-km break along part of the Denali fault. Along the fault, we observed offset features [supporting online material (SOM) Text, table S1], extensional and contractional stepovers, en-echelon fissures, and Riedel shears in snow, glacier ice, and sediment. Dislocations were primarily dextral, with a smaller amount of vertical slip. At the eastern limit of the ruptures on the Denali fault, the rupture stepped southeastward onto the Totschunda fault across a complex, 14-km-long transfer zone. The Denali fault did not break east of this intersection. The transfer zone is characterized by a series of right-stepping fault segments connected by north-striking, east-side-up normal faults with displacements up to 2.7 m. The surface ruptures, mostly in a narrow zone of dextral offset, extend a total of 76 km southeastward along the Totschunda fault (Fig. 3).

The distribution of surface slip is asymmetrical along the Denali and Totschunda faults (Fig. 3B). We infer that our measurements of surface offsets are lower bounds for the total offset across the fault, due to unrecognized drag across the fault zone (SOM Text). Thus, the actual slip distribution is probably near the solid line through the largest values shown on Fig. 3B. Right-lateral offset on the Denali fault dominates the slip distribution, averaging 5.3 m (*21*). Slip on the fault can be broadly subdivided into four sections, with average inferred slip of 2.7, 5.3, 4.7, and 6.8 m from west to east. The largest measured horizontal offset was 8.8 m about 190 km east of the epicenter. The rupture stops abruptly at both ends. Offsets along the Totschunda fault (average, 1.5 m; maximum, 2.1 m) are modest and more symmetrical. The vertical slip along the Denali and Totschunda ruptures has the same distribution as the horizontal (fig. S1). The largest vertical offsets, regardless of the sense of slip, are associated with the largest horizontal offsets.

Thrusting on the Susitna Glacier fault raised the north side relative to the south. Along the 40-km rupture, we measured scarp heights (average, 1.4 m; maximum, 4 m) (SOM Text, table S1). Two observations of fault dip where it crossed small valleys were 10° and 25°, and if the steeper 25° dip is used for calculating fault offset (*22*), there was about 3.3 m total dip-slip on the Susitna Glacier fault. The initial thrusting observed seismically represents the Susitna Glacier fault, with the hypocentral location implying that rupture was bilateral. The focal mechanism has a steeper 48° dip than the surface dips of 10° to 25°. Thus, the dip decreases as the fault approaches the surface—typical of thrusts associated with strike-slip systems (*23*).

Distribution of moment release. Global positioning system (GPS) measurements had been made before the earthquake, and 26 sites were resurveyed to estimate surface displacements resulting from the earthquake (*24*, *25*) (Fig. 4). Using a five-plane approximation for the fault geometry, divided into a grid of subfaults (*26*), we inverted the GPS data to determine the distribution of fault slip. The fault model used here does not include the Susitna Glacier fault, as most GPS sites are weakly sensitive to slip on that fault. Smoothing is used to regularize the inversion. Models with more and less smoothing show the same general features. We show the along-strike geodetic moment (Fig. 3C) as a summation of model slip times fault area over all depths, as this quantity does not change much regardless of smoothing. The inferred seismic moment is high in two sections, one centered about 70 km east of the hypocenter and another centered about 200 km east of the hypocenter. Total seismic moment is equivalent to M_W 7.9.

Strong-motion seismograms (*27*) recorded at distances of 3 to 300 km from the fault rupture and seismograms at teleseismic distances show that rupture occurred first on the Susitna Glacier fault and then proceeded from west to east on the Denali and Totschunda faults. Seismograms show that slip and energy release were heterogeneous along the Denali fault. We identified three subevents by modeling and inverting the strong-motion records (Fig. 5). The first subevent had an M_W of 7.2 and is associated with thrusting on a nearly east-west striking fault near the hypocenter. It is not resolvable whether there was strike-slip motion on the Denali fault simultaneous with this thrusting on the Susitna Glacier fault.

The second and third subevents were identified by inverting the strong-motion waveforms after the first subevent to determine the right-lateral strike-slip moment release along the Denali and Totschunda faults (*28*–*30*) (Fig. 5). The second subevent was located 50 to 100 km east of the hypocenter (Figs. 2 and 3), where the surface offsets increase to over 6 m. This subevent was located near where the Trans Alaska Pipeline crosses the Denali fault and was equivalent to about M_W 7.3. The ground-motion pulse observed at the station nearest the fault, Pump Station 10 (PS10) (Fig. 5), was produced by this subevent, which was centered on the portion of the fault closest to this station. The S-wave and Love wave arrivals for this subevent are prominent on the Anchorage and Fairbanks records (Fig. 5, A and B).

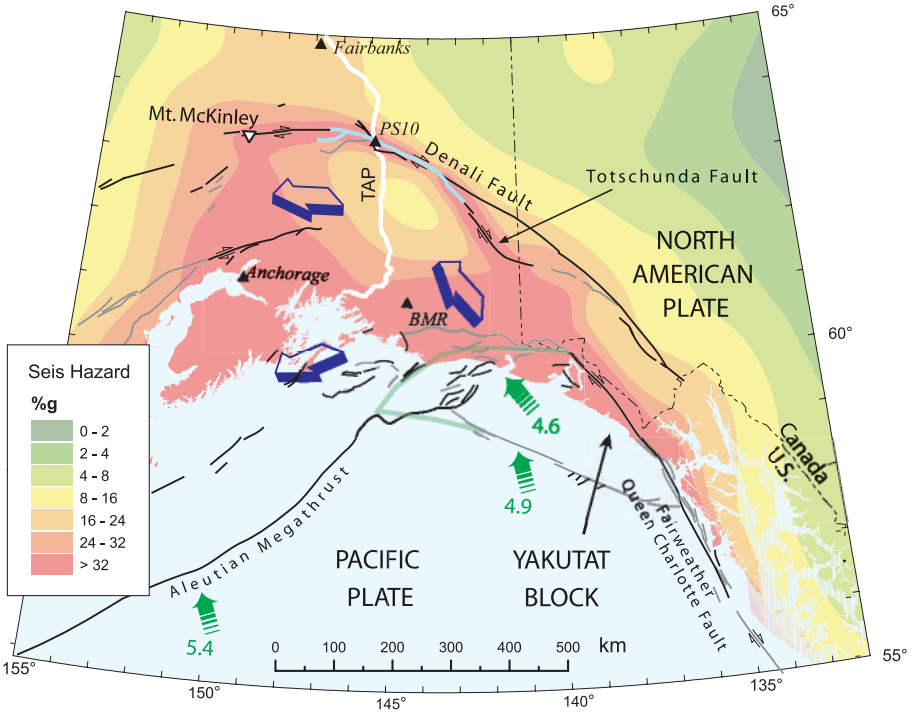

Fig. 1. Plate tectonic setting of southern Alaska and major tectonic elements. The Pacific and North American plates converge at 5.4 cm/year beneath Anchorage (*53*), and the Yakutat block collides with North America independently. Plate motion is indicated by green arrows. Blue open arrows schematically show lateral movement of broad region south of the Denali fault. Blue line, surface rupture. The probabilistic seismic hazard is shown by peak ground acceleration with 10% probability of exceedance in 50 years (*14*). TAP, Trans Alaska Pipeline. Triangles, station locations in Fig. 5. Black lines, Quaternary faults; gray lines, Neogene faults.

The third subevent is located about 140 to 220 km east of the hypocenter (Figs. 2 and 3). Strong-motion stations southeast of the epicenter, such as BMR, show a large displacement pulse from this subevent (Fig. 5C). This subevent had the largest seismic moment, equivalent to about M_W 7.6, and was located in the region with the maximum surface offset of 8.8 m (Fig. 3B). The total seismic moment from the strong-motion inversion corresponds to M_W 7.8. The best-fitting inversion requires a high rupture velocity, about 3.5 km/s, between subevents 2 and 3. The moment distribution is similar to that determined from other seismic inversions (*31*–*33*).

The locations of the larger surface offsets correlate with the locations of high moment release found in the inversions of geodetic and strong-motion data (Fig. 3). All three data sets show increased slip 50 to 100 km and 150 to 230 km east of the epicenter, although the surface offset data do not show as pronounced of a decrease in slip between these areas as the geophysical data indicate. The seismic moments calculated from our strong-motion inversion (M_W 7.8) and from the teleseismic waveforms (*31*) (M_W 7.9) agree well with the moment calculated from the surface slip (*34*) (M_W 7.8) and the geodetic data (M_W 7.9).

Surface slip and moment release diminished sharply southeast of the Denali-Totschunda fault junction. Observations of right-stepping faults and large vertical offsets in the 14° bend at the junction suggest that the Denali-Totschunda junction is a complex feature. The geometric complexity and the drop in fault slip suggest that the junction was a barrier to rupture propagation. Available slip-rate evidence suggests that the Totschunda fault is more active than the eastern Denali fault, and this relation coupled with high rupture velocity may have favored rupture propagation on the Totschunda fault more than the eastern Denali fault (*35*).

Landslides and Liquefaction

The earthquake triggered thousands of landslides ranging in size from a few cubic meters to tens of millions of cubic meters. Most impressive were several giant rock avalanches that spilled onto the McGinnis, Black Rapids, and West Fork Glaciers in the Alaska Range. The largest of these involved about 30 million m^3 of rock and ice that collapsed off the north and east flanks of McGinnis Peak and then traveled about 10 km down the McGinnis Glacier at high speed. The long runout of this landslide is remarkable considering that the glacial surface on which it moved had an average slope of only 5°.

The landslides were concentrated in a narrow band 30 km wide along the surface rupture of the faults and in the hanging wall of the Susitna Glacier fault (Fig. 4). An earthquake of this magnitude would be expected to trigger landslides over a broad region extending perhaps 250 km from the fault (*36*), so the moderate concentration of landslides suggests a deficiency of high-frequency shaking. The largest landslides were concentrated in the area of the first two subevents of the earthquake (Fig. 4). The eastern third subevent produced the greatest slip but fewer landslides. The eastern topography is still very steep and would have been expected to produce more landslides in this area of greater fault slip if accelerations were larger where slip was larger.

Liquefaction features were observed at a greater distance from the zone of concentrated landslides for Denali, whereas typically earthquakes show landslides and liquefaction features in the same area. In addition, the liquefaction features were more extensive and more severe, i.e., they had larger associated lateral displacements and vertical settlements, to the east in the area of the third subevent. The extensive liquefaction may be attributed to the high long-period energy in

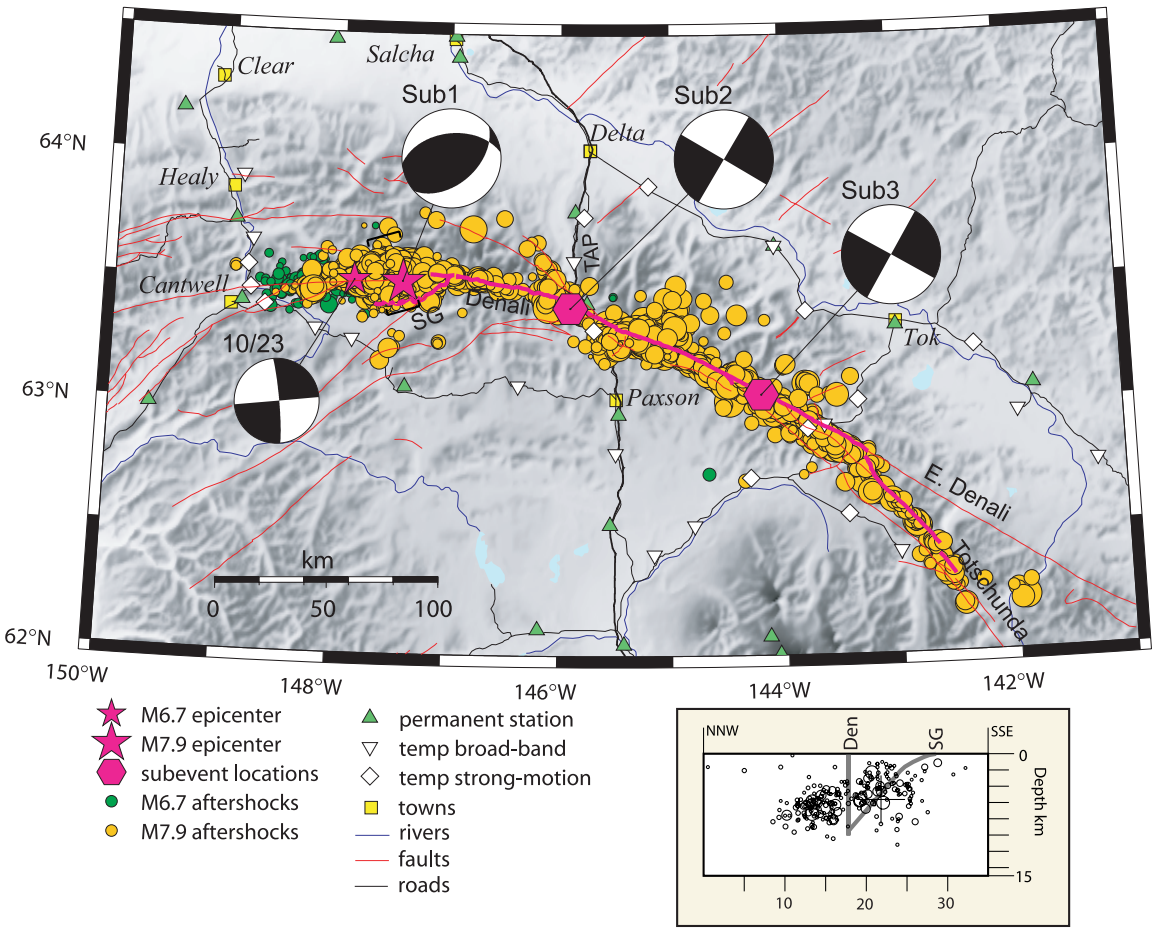

Fig. 2. Locations of principal earthquakes and aftershocks. Stars show the hypocenters of the 23 October M_W 6.7 and 3 November M_W 7.9 earthquakes, with double-difference relocated aftershocks shown in green and orange, respectively. Focal mechanisms show the first motion solution for the M_W 6.7 earthquake and the 3 subevents (sub1 to -3) determined for the M_W 7.9 earthquake. Mapped surface rupture shown as heavy magenta line; red lines indicate other faults. The inset cross section shows schematic faults and $M_L \geq 2.5$ aftershocks in the bracketed zone across the Susitna Glacier (SG) thrust, inferred to splay off the Denali (Den) fault. Cross, mainshock.

this large magnitude strike-slip event, which can produce large volumetric strain and high peak velocity without associated high peak acceleration.

Aftershocks

Along most of the fault, the aftershocks were concentrated along the surface rupture (Fig. 2). Most aftershocks were located above 10 km depth, suggesting rupture did not extend much deeper. The location algorithm that we used produces precise relative hypocenters (*37*), but absolute earthquake depths remain poorly determined with the sparse permanent network (*38*). The aftershocks represent minor slip on fault zones and distributed fractures in response to the stress perturbation. Near the mainshock hypocenter (Fig. 2 cross section), aftershocks south of the Denali fault roughly correspond to the inferred position of the Susitna Glacier fault, based on its surface trace, shallow dip (15° to 25°) at the surface, and the focal mechanism of subevent 1. The aftershocks on the north side may represent seismicity on south-dipping thrust faults of the Alaska Range. Elsewhere along the rupture, some off-fault aftershocks are associated with splay faults.

There were few large aftershocks of the Denali Fault event, and the sequence decayed relatively quickly. Statistical parameters have been computed (*39*, *40*). The magnitude distribution of the aftershock sequence, with the largest aftershock M_W 5.8, is fit by b = 1.2, which is slightly high compared to generic California b = 0.9 (*40*). The aftershock productivity is fit by a = –3.4, which is low compared to a ~ 1.7 in California and New Zealand (*40*, *41*). The parameters are similar for aftershocks of the M_W 6.7 event. Relatively low aftershock productivity might be characteristic of the region or of rupture of a major, well-developed fault. Another possibility is that the aftershock scaling relations may break down for long strike-slip ruptures, but the similarly low productivity of the M_W 6.7 foreshock sequence argues against this explanation.

Directivity and Remote Effects

The effects of rupture directivity are particularly striking for the Denali fault event (Fig. 5). For subevent 3, stations at azimuths over 90° from the rupture propagation direction, such as Fairbanks and Anchorage, do not show distinct arrivals. Subevent 3 produces a strong displacement pulse at BMR, at an azimuth about 55° closer to the propagation direction. The difference at stations only 55° apart in azimuth suggests high rupture velocity for subevent 3, confirmed by our inversion. Station PS10 only records a pulse from subevent 2 and not from the largest slip subevent, which is propagating away from this station (Fig. 5E).

The long unilateral rupture produced strong directivity in both the teleseismic S-waves and the surface waves. The energy flux of the teleseismic S-waves recorded at North American stations was four to five times greater than the energy flux recorded at European and Asian stations at the same distance in the back-azimuth direction (*42*, *43*). People reported feeling ground shaking as far as 3500 km from the epicenter (*44*), indicating strong focusing of surface waves in the propagation direction. Seiches were observed as far away as Louisiana (*45*) and lasted 5 to 30 min, rocking boats and breaking moorings. Remote effects were influenced by local features such as the Seattle basin, which amplified surface waves (*46*).

The Denali fault event triggered bursts of local earthquake activity to distances as great as 3660 km. Of seven documented instances of triggered seismicity, six are located in areas of volcanism or geothermal activity: (i) the Katmai volcanic field in Alaska (700 to 735 km), (ii) Mount Rainier in central Washington (3108 km), (iii) Yellowstone caldera in Wyoming (3100 to 3150 km), (iv) the Geysers geothermal field in northern California (3120 km), (v) Long Valley caldera in east-central California (3454 to 3460 km), and (vi) the Coso geothermal field in southeastern California (3660 km). The other site is along the Wasatch fault zone, central Utah. The triggered seismicity developed as rapid sequences of small [M_L (local magnitude) < 3] earthquakes that persisted for durations rang-

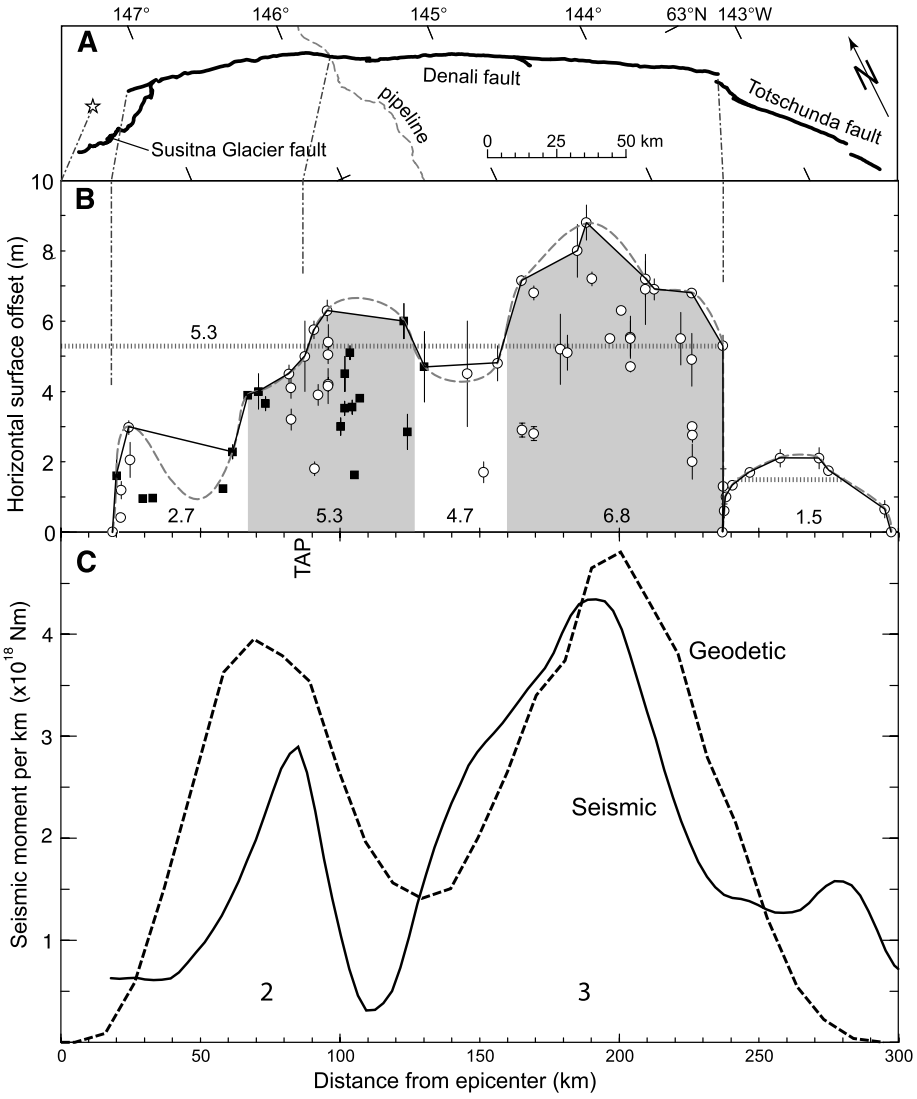

Fig. 3. Along-fault distribution of horizontal slip and moment release, from geologic and geophysical data. (**A**) Map view of surface rupture; star, epicenter. (**B**) Measured dextral offsets at nonglacier (circles) and glacier (filled squares) sites. Inferred surface slip distribution is defined by straight line segments connecting the largest slip values (SOM Text). Numbers indicate average slip of the maximum values in each segment and are averages for Denali and Totschunda faults. Dashed line shows an alternate smoothed curve. (**C**) Strike-slip moment per kilometer along strike derived from inversion of geodetic (dashed line) and strong-motion (solid line) data. Combined observations show two areas of high moment release (subevents 2 and 3). TAP, Trans Alaska Pipeline.

ing from several minutes in the case of Mount Rainier to days in the case of Yellowstone.

Yellowstone caldera, nearly in line with the rupture propagation direction, produced the most energetic response. The triggered activity ($-1 < M_L < 2.7$) began with the arrival of the first surface waves, which had peak dynamic stresses of ~200 kPa at a period of 20 s. The initial activity at Yellowstone was vigorous with over 130 earthquakes occurring in spasmodic bursts during the first four hours. Seismicity slowed to ~35 events per day after a few days, but swarms continued to occur for at least 10 days. The triggered earthquakes were distributed over the entire volcanic field in contrast to the usual seismicity, and were accompanied by unusual variations in geothermal activity (*47*).

All triggered sites except for Katmai lie in the rupture propagation direction, which further underscores the importance of directivity. Katmai is the only site with a recognized response in a back-azimuth direction, and it is the only one of the many active Alaskan volcanoes that showed triggered seismicity. Veniaminof and Wrangell volcanoes showed decreases in seismicity rate, starting several days afterward (*48*).

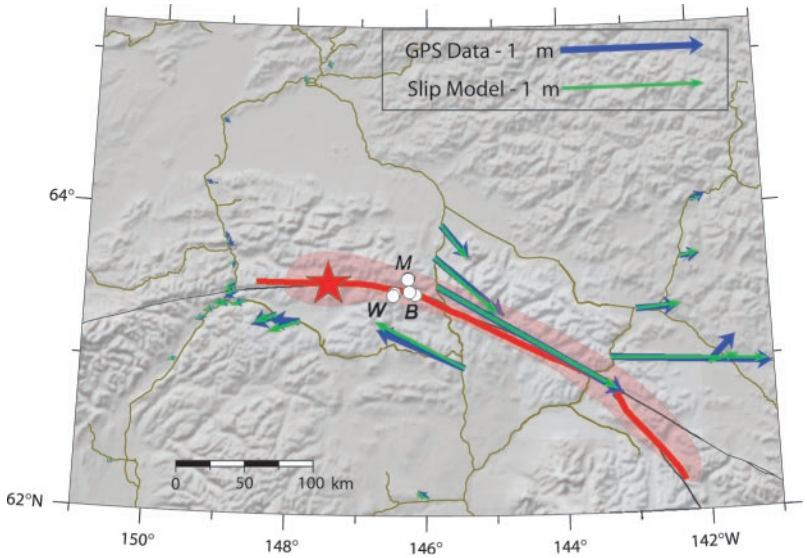

Fig. 4. GPS observations of coseismic displacement (blue arrows) and modeled displacement (green arrows) obtained by inversion on simplified fault (red line). Shaded red region shows zone of concentrated landslides. White dots indicate sites of major landslides: M, McGinnis Peak; W, West Fork; B, Black Rapids.

Implications for Seismic Hazards

The Denali fault event is larger than other recent well-recorded large damaging earthquakes, such as Chi-chi, Taiwan (M_W 7.6) and Izmit, Turkey (M_W 7.4). It is similar to the 1906 San Francisco (M_W 7.8) and 1857 Fort Tejon (M_W 7.9) earthquakes on the San Andreas Fault in California (*49*, *50*), in that all three events had similar magnitudes and rupture lengths.

Previous studies have inferred that large surface ruptures may have relatively weak ground shaking at short and intermediate periods because the effective slip velocity near the surface is low (*51*). The largest recorded acceleration for the Denali Fault event, 0.34*g* at PS10, is similar to the 0.2 to 0.3*g* peak accelerations observed at near-field sites for the M_W 7.4 Izmit earthquake but much lower than for

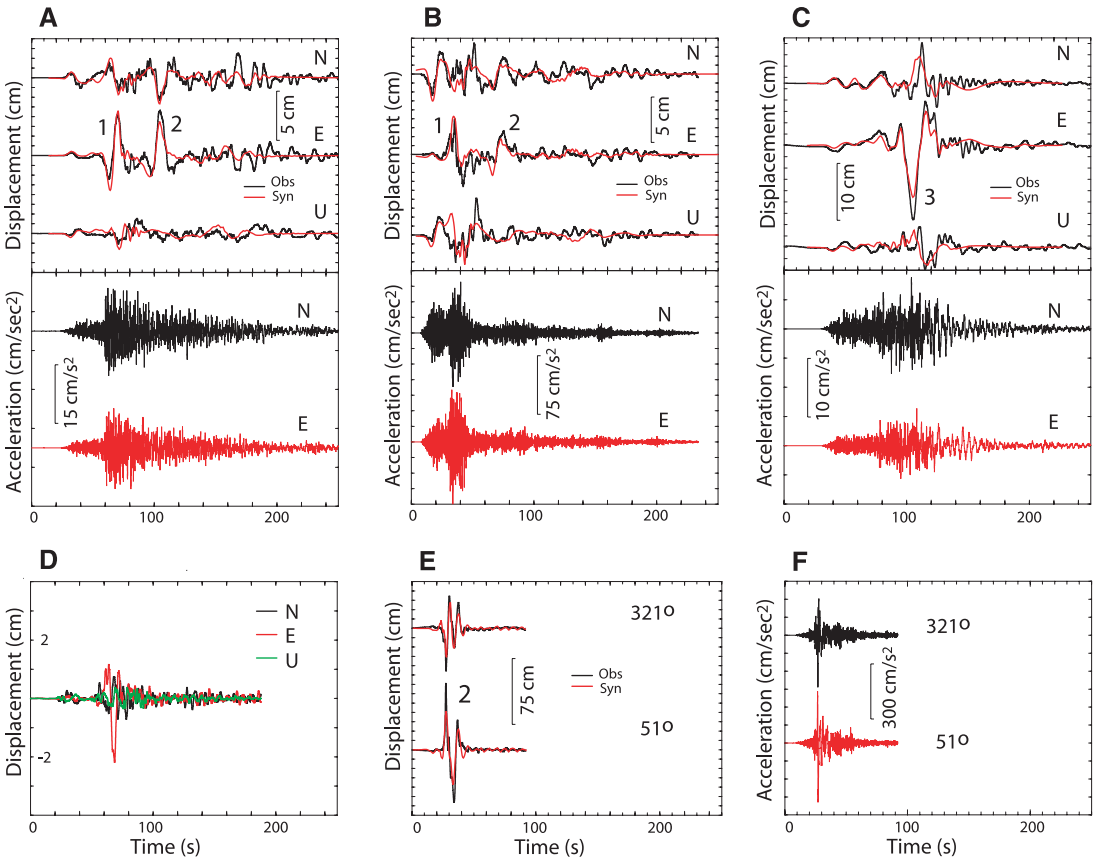

Fig. 5. Strong-motion modeling. Observation of subevents (1 to 3) is highly dependent on azimuth. (**A**) Anchorage, (**B**) Fairbanks, and (**C**) BMR records. (**D**) M_W 6.7 event, recorded at Anchorage. (**E** and **F**) PS10 record, 3 km from rupture, recorded with a 0.1 Hz high-pass filter so that it does not show static displacement (*27*). Site locations are shown in Fig. 1. Traces begin at the trigger times. Stations recorded north (N), east (E), and vertical (U) components, except PS10, which recorded 321° and 51° components.

the M_W 7.3 Landers earthquake, where the observed 0.8*g* peak acceleration was enhanced by directivity effects. The acceleration at PS10 is less than might be expected for a M_W 7.9 earthquake, and, considered together with the paucity of landslides, might imply relatively low strong motion near the rupture. However, it may not be representative of the maximum near-field accelerations produced by this earthquake, because the PS10 waveforms are primarily from subevent 2. It should be emphasized that the near-field velocity pulse at PS10 is quite large, 114 cm/s (high-pass filtered record). This is similar to the large peak velocities found at near-field stations located down-rupture from the epicenter of other large earthquakes.

The Denali fault earthquake produced long-duration, long-period motion, which is important in causing damage to tall buildings and bridges because it can shake them near their long natural periods. The longer duration and increased long-period energy in the M_W 7.9 event compared with the M_W 6.7 event is evident in their records (Fig. 5, A and D). The M_W 6.7 event has a simple displacement pulse with a period of about 10 s, whereas the M_W 7.9 event has an overall duration of shaking of about 140 s, with individual subevent displacement pulses having periods of about 20 to 30 s. Engineering models for major structures should consider the large directivity effect exhibited by the Denali fault earthquake, which compresses and amplifies the displacement pulse from a long rupture.

During the Denali fault event, rupture of a relatively inactive secondary thrust evolved into a major strike-slip fault rupture—the opposite of what might be expected. This scenario could also happen in southern California, where thrust faults and strike-slip faults intersect, increasing the magnitude. The magnitude of a major earthquake would depend on how the dynamic rupture progressed. Consideration of a range of earthquake magnitudes and directivity effects may be most appropriate for hazard planning.

The concomitant widening of a thrust belt on the north side of the Alaska range may indicate slip is transferred to thrust faults in a large region straddling the Denali fault near the epicenter. The correlation between the location of the Susitna Glacier fault and a slight (12°) bend in the Denali fault suggests the thrust fault may be associated with movement around the bend.

The Denali fault ruptured beneath the Trans Alaska pipeline, and surveys indicate a total of about 5.5 m of dextral slip. The pipeline, designed to withstand 6.1 m of dextral slip at the fault crossing (*12*), withstood the earthquake with little damage and no spillage of oil. This success demonstrates the value of preconstruction geotechnical studies in earthquake risk mitigation.

The Denali fault event increased the Coulomb stress by over 400 kPa on the eastern Denali and eastern Totschunda faults and by up to 80 kPa on the western Denali fault (*18*), bringing those fault segments closer to failure. The likelihood of rupture depends on the previous earthquake history, though prior events on these faults are undated. The Totschunda fault may be close to failure because 20 km southeast of the 2002 surface rupture a tephra that erupted around AD 735 (*53*) was undisturbed across the fault (*7*). Thus, with a long-term slip rate on the order of 0.5 to 1 cm/year (*7*, *8*), this segment of the fault may have already accumulated 5 to 10 m of strain.

References and Notes

1. G. Plafker, J. C. Moore, G. R. Winkler, *The Geology of North America*, **G-1**, 389 (Geological Society of America, Boulder, CO, 1994).
2. J. C. Lahr, G. Plafker, *Geology*, **8**, 483 (1980).
3. P. J. Haeussler, R. L. Bruhn, T. L. Pratt, *Geol. Soc. Am. Bull.* **112**, 1414 (2000).
4. D. H. Richter, N. A. Matson, *Geol. Soc. Am. Bull.* **82**, 1529 (1971).
5. E. E. Thoms, thesis, Univ. of Alaska Fairbanks, (2000).
6. K. D. Ridgeway, J. M. Trop, W. J. Nokleberg, C. M. Davidson, K. R. Eastham, *Geol. Soc. Am. Bull.* **114**, 1480 (2002).
7. G. Plafker, T. Hudson, D. H. Richter, *U.S. Geol. Surv. Circ.* **751-B**, B67 (1977).
8. H. J. Fletcher, thesis, Univ. of Alaska Fairbanks (2002).
9. G. Plafker, L. Gilpin, J. Lahr, in (*1*), pl. 12.
10. K. E. Sieh, L. S. Cluff, *Geol. Soc. Am. Abstr. Prog.* **7**, 423 (1975)
11. Displacements of 7.5 to 15 m (*10*) may include creep or multiple offsets. G. Plafker (unpublished data) found well-constrained offsets of 6 to 8 m in the epicentral region of the M_W 6.7 event.
12. L. S. Cluff, D. B. Slemmons, *Eos* **83**, abstr. S72F-1329 (2002).
13. Alyeska Pipeline Service Company (APSC), Design Basis DB-180 (APSC, Fairbanks, AK, ed. 4, rev. 2, 2002).
14. R. L. Wesson, A. D. Frankel, C. S. Mueller, S. C. Harmsen, *U.S. Geological Survey Geologic Investigations map I-2679*, 2 sheets (1999).
15. A foreshock is located within a distance equivalent to its rupture length (thus, within about 30 to 40 km for the M_W 6.7 foreshock) of the mainshock epicenter within a time frame when the foreshock's aftershocks are clearly above background level.
16. R. A. Harris, *J. Geophys. Res.* **103**, 24347 (1998).
17. R. S. Stein, *Nature* **402**, 605 (1999).
18. G. Anderson, C. Ji, *Geophys. Res. Lett.* **30**, 1310 (2003).
19. A. Ziv, A. Rubin, *J. Geophys. Res.* **105**, 13631 (2000).
20. T. Parsons, R. S. Stein, R. W. Simpson, P. A. Reasenberg, *J. Geophys. Res.* **104**, 20183 (1999).
21. Calculating the average under the straight-line curve on Fig. 4B.
22. The steeper dip yields a smaller estimate of fault slip.
23. A. Sylvester, *Geol. Soc. Am. Bull.* **100**, 1666 (1988).
24. Analysis used GIPSY software (*32*), with fixed precise orbits from the International GPS Service. Displacements were estimated using the time series of preearthquake measurements and the first week of postearthquake data. For sites near the M_W 6.7 foreshock, we estimated displacements for the M_W 7.9 using GPS measurements made between the two earthquakes and after the M_W 7.9.
25. J. F. Zumberge, M. B. Heflin, D. C. Jefferson, M. M. Watkins, F. H. Webb, *J. Geophys. Res.* **102**, 5005 (1997).
26. R. E. Reilinger *et al.*, *Science* **289**, 1519 (2000).
27. Data from USGS NSMP stations at Fairbanks and Valdez, and University of Alaska Fairbanks stations at Anchorage, BMR, and two temporary sites deployed after the M_W 6.7 event. PS10 records were provided by Alyeska. In Fig. 5, Anchorage and Fairbanks records are high-pass filtered at 70 s, BMR record is high-pass filtered at 100 s, and PS10 record is high-pass filtered at 10 s. W. Ellsworth determined the filter characteristics for PS10 records.
28. Green's functions were calculated by frequency-wavenumber methods (*29*) with an Alaska model (*30*). For modeling PS10 records, we added a near-surface sediment layer. A 6-km source depth was used in the strong-motion inversion.
29. C. K. Saikia, *Geophys. J. Int.* **118**, 142 (1994).
30. J. C. Lahr, R. A. Page, C. D. Stephens, K. A. Fogleman, *Bull. Seism. Soc. Am.* **76**, 967 (1986).
31. M. Kikuchi, Y. Yamanaka, "Source rupture processes of the central Alaska earthquake of Nov. 3, 2002, inferred from teleseismic body waves (+ the 10/23 M6.7 event)," EIC Seismological Note No. 129, revised 5 November 2002. Available from the Earthquake Information Center, University of Tokyo, at http://www.eic.eri.u-tokyo.ac.jp/EIC/EIC_News/021103AL-e.html.
32. C. Ji, D. Helmberger, D. Wald, *Eos* **83**, abstr. S72F-1344 (2002).
33. D. Dreger *et al.*, *Eos* **83**, abstr. S72F-1343 (2002).
34. Assuming surface values extend to 10-km depth, M_W values for the three rupture segments are 7.3, 7.7, and 7.1, for total M_W of 7.8.
35. H. S. Bhat, R. Dmowska, J. R. Rice, N. Kame, *Eos* **83**, abstr. S72F-1364 (2002).
36. D. K. Keefer, *Geol. Soc. Am. Bull.* **95**, 406 (1984).
37. F. Waldhauser, W. L. Ellsworth, *Bull. Seismol. Soc. Am.* **90**, 1353 (2001).
38. These double-difference hypocenters with permanent network data have average horizontal and vertical errors of 2 to 3 km. Errors vary along the rupture zone, depending on the station distribution.
39. On the basis of 65 $M_L \geq 5$ California aftershock sequences, the aftershock rate is formulated (*41*) as $10^{[a + b(M_m - M)]} * (t + c)^{-p}$, where t is time, M is aftershock magnitude, M_m is mainshock magnitude, and a, b, c, and p are constants.
40. P. A. Reasenberg, L. M. Jones, *Science* **243**, 1173 (1989).
41. D. Eberhart-Phillips, *Bull. Seismol. Soc. Am.* **88**, 1095 (1998).
42. J. Boatwright, personal communication.
43. A. A.Velasco, W. I. Sevilla, C. Flores, C. J. Ammon. *Eos* **83**, abstr. S72F-1341 (2002).
44. J. F. Cassidy, G. C. Rogers, A. Bird, T. L. Mulder, *Eos* **83**, abstr. S72F-1354 (2002).
45. F. D. Roylance, *Baltimore Sun*, 29 November 2002, p. Telegraph 1A.
46. A. Barberopoulou *et al.*, *Eos* **83**, abstr. S72F-1355 (2002).
47. S. Husen, S. Nava, R. B. Smith, F. Terra, K. Pankow, *Eos* **83**, abstr. S72F-1356 (2002).
48. S. R. McNutt, J. J. Sanchez, S. C. Moran, J. A. Power, *Eos* **83**, abstr. S72F-1353 (2002).
49. L. B. Grant, K. E. Sieh, *Bull. Seism. Soc. Am.* **83**, 619 (1993).
50. W. Thatcher, G. Marshall, M. Lisowski, *J. Geophys. Res.* **102**, 5353 (1997).
51. P. G. Somerville, A. Pitarka, T. Kagawa, *Seismol. Res. Lett.* **73**, 260 (2002).
52. J. F. Lerbekmo, J. A. Westgate, D. G. W. Smith, G. H. Denton, *Quat. Stud.* **13**, 203 (1975).
53. D. C. DeMets, R. G. Gordon, D. F. Argus, S. Stein, *Geophys. Res. Lett.* **21**, 2191 (1994).

54. We thank B. Atwater, J. Boatwright, D. Schwartz, R. Stein, M. L. Zoback, and anomymous referees for constructive reviews; D. Wald, R. Wesson, W. Ellsworth for useful discussions; and D. McNamara, C. Stephens, N. Biswas, A. Martirosyan, and U. Dutta for data.

Supporting Online Material

www.sciencemag.org/cgi/content/full/300/5622/1113/DC1
SOM Text
Fig. S1
Table S1

23 January 2003; accepted 4 April 2003